An Apolipoprotein AI Mimetic Peptide: Membrane Interactions and the Role of Cholesterol[†,‡]

Richard M. Epand,[*,§] Raquel F. Epand,[§] Brian G. Sayer,[§] Giuseppe Melacini,[§] Mayakonda N. Palgulachari,[||] Jere P. Segrest,[||] and G. M. Anantharamaiah[||]

Departments of Biochemistry and Chemistry, McMaster University, Hamilton, ON L8N 3Z5, Canada, and Departments of Medicine, Biochemistry, and Molecular Genetics and The Atherosclerosis Research Unit, University of Alabama at Birmingham, Birmingham, Alabama 35294

Received January 30, 2004; Revised Manuscript Received March 3, 2004

ABSTRACT: The 18-amino acid amphipathic helical peptide Ac-DWFKAFYDKVAEKFKEAF-NH_2 promotes the separation of cholesterol from the phospholipid, resulting in the formation of cholesterol crystallites, even at mole fractions of cholesterol as low as 0.3. The peptide exerts a greater degree of penetration into membranes of pure phosphatidylcholine in the absence of cholesterol than into bilayers of phosphatidylcholine and cholesterol. The circular dichroism spectrum of the peptide in buffer indicates that it self-associates, leading to the formation of structures with higher helical content. However, in the presence of lipid, the peptide remains helical over a larger concentration range. The peptide undergoes a thermal transition on heating. Cholesterol has little effect on the secondary structure of the peptide; however, increased Trp emission intensity in the absence of cholesterol indicates a deeper penetration of the helix upon removal of cholesterol from the membrane. The results with these model systems demonstrate changes in peptide−lipid interactions that may be related to the observed biological properties of this peptide.

There is a growing body of evidence which shows that certain apo A-I mimetic, class A amphipathic helical peptides can be used to inhibit atherosclerosis (*1*). It has been shown that either intraperitoneal administration of a class A amphipathic helical peptide (4F)[1] or the oral administration of peptide 4F synthesized from all-D amino acids inhibits atherosclerosis in dyslipidemic mouse models without altering plasma cholesterol levels (*2*, *3*). There are at least two processes that can be influenced by the apo A-I mimetic, class A amphipathic helical peptides that would protect against atherosclerosis. One of these is the well-established role of HDL in "reverse" transport of cholesterol from peripheral tissues to the liver for excretion (*4*), and the other is the inhibition of inflammatory processes (*5*).

Elevated levels of cholesterol are a risk factor in the development of atherosclerosis. Higher levels of cholesterol in the plasma membrane of cells may inhibit the interaction of class A peptides with these membranes and thus prevent their protective action. Resonance energy transfer studies indicate that cholesterol modulates the insertion of the tryptophan residue of the amphipathic helical class A peptide, *N*-acetyl-18A-amide, with bilayers of phosphatidylcholine (*6*, *7*). Peptide 4F was found to be the most active among a series of analogues of *N*-acetyl-18A-amide in inhibiting LDL-induced monocyte chemotatic activity (*8*). This peptide, with an Ac-DWFKAFYDKVAEKFKEAF-NH_2 sequence, has the potential to form an amphipathic helix (Figure 1). In this work, we investigate the interaction of amphipathic helical peptide 4F with phosphatidylcholine, either in the presence or in the absence of cholesterol. In addition, we demonstrate the ability of the peptide to promote the formation of cholesterol-rich domains.

MATERIALS AND METHODS

Lipids. Lipids used in this study were obtained from Avanti Polar Lipids (Alabaster, AL). The purity of the phospholipids was verified by measuring the cooperativity and temperature of the phase transition using DSC.

Peptide Synthesis. Peptide 4F was synthesized by the solid phase method with a Protein Technologies PS-3 automatic peptide synthesizer using the procedures described previously (*8*). The peptide was purified using a preparative HPLC system (Beckman Gold), and the purity of the peptides was ascertained by mass spectral analysis and analytical HPLC as previously reported (*8*).

Concentrations of the Peptide and Lipid. The concentrations of peptide solutions in buffer were determined spectrophotometrically using the absorbance at 280 nm and an

[†] This work was supported by Grant MT-7654 from the Canadian Institutes of Health Research and Grants HL 34343 and RO1 HL 65663 from the U.S. National Institutes of Health.

[‡] G.M.A. is the principal in Bruin Pharma, a startup biotech company.

* To whom correspondence should be addressed. E-mail: epand@mcmaster.ca.

[§] McMaster University.

[||] University of Alabama at Birmingham.

[1] Abbreviations: apo A-I, apo A-II, and apo C-II, plasma apolipoproteins A-I, A-II, and C-III, respectively; HDL, high-density lipoprotein; 4F, Ac-DWFKAFYDKVAEKFKEAF-NH_2; PC, phosphatidylcholine; PO, 1-palmitoyl-2-oleoyl; SO, 1-stearoyl-2-oleoyl; LPC, lysophosphatidylcholine; DPH-PC, 2-[3-(diphenylhexatrienyl)propanoyl]-1-hexadecanoyl-*sn*-glycero-3-phosphocholine; CP, cross polarization; DP, direct polarization; MAS, magic angle spinning; NOE, nuclear Overhauser enhancement; NOESY, nuclear Overhauser enhancement spectroscopy; MLV, multilamellar vesicle; LUV, large unilamellar vesicle; SUV, small unilamellar vesicle; DSC, differential scanning calorimetry; CD, circular dichroism; T_m, transition temperature; ΔH_{cal}, calorimetric enthalpy; ΔC_p, change in heat capacity at constant pressure.

10.1021/bi049786u CCC: $27.50
Published on Web 04/09/2004

Ac-D**W**F**K**A**FY**DKVAEK**F**KEA**F**-NH_2

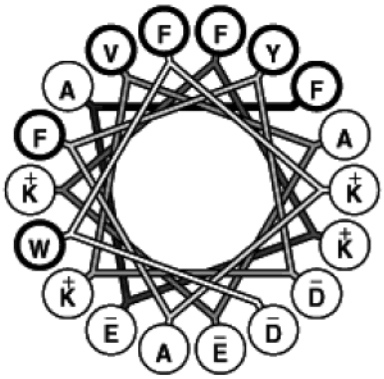

FIGURE 1: Helical wheel representation of antiatherogenic 4F. The primary structure is given above the wheel diagram. The aromatic amino acids are shown in bold. In the helical wheel diagram, the hydrophobic amino acids are shown in bold circles. The plus and minus signs denote the charge on the amino acid at neutral pH.

extinction coefficient of 6800 cm^{-1} M^{-1}, calculated from the Tyr and Trp content. The phospholipid concentration was determined by phosphate analysis (*9*).

Preparation of Samples for DSC and NMR Experiments. Phospholipid and cholesterol were dissolved in a chloroform/methanol mixture (2/1, v/v). For samples containing peptide, an aliquot of a solution of the peptide in methanol was added to the lipid solution in the chloroform/methanol mixture. The solvent was then evaporated under a stream of nitrogen with constant rotation of a test tube so that a uniform film of lipid could be deposited over the bottom third of the tube. Last traces of the solvent were removed by placing the tube under high vacuum for at least 2 h. The lipid film was then hydrated with 20 mM PIPES, 1 mM EDTA, and 150 mM NaCl with 0.002% NaN_3 (pH 7.40) and suspended by intermittent vortexing and being heated to 50 °C for 2 min under argon. Samples used for NMR analysis were hydrated with the same buffer made in either regular water at pH 7.4 or ^2H_2O and adjusted to a pH meter reading of 7.0 (pD 7.4). The samples used for NMR were incubated for 24 h at 4 °C to allow conversion of anhydrous cholesterol crystals to the monohydrate form. For the NMR measurements, the samples were spun in an Eppendorf centrifuge at room temperature. The resulting hydrated pellet was transferred to an 12 μL capacity spherical insert of a 18 mm × 4 mm ZrO_2 rotor, attempting to pack the maximal amount of lipid into the rotor while keeping it wet.

Differential Scanning Calorimetry (DSC). Measurements were taken immediately after sample preparation using a nano differential scanning calorimeter (Calorimetry Sciences Corp., American Fork, UT). The scan rate was 2 °C/min, and there was a delay of 5 min between sequential scans in a series to allow for thermal equilibration. The features of the design of this instrument have been described previously (*10*). DSC curves were analyzed by using the fitting program, DA-2, provided by Microcal Inc. (Northampton, MA) and plotted with Origin, version 5.0.

Centrifugation Assay for Membrane Binding of 4F. The fraction of peptide bound to the lipid after three heating and cooling cycles between 0 and 100 °C was determined by separating the sample by centrifugation. The vesicles with bound protein were pelleted at 200000*g* for 90 min at 25 °C. A clear supernatant was separated from the solid pellet and assayed for protein by absorption at 278 nm. The absorption of a blank was subtracted, and a baseline, set at 350 nm for each sample, was used to correct for residual scattering. In addition, the amount of lipid in both pellet and supernatant fractions was determined by phosphate analysis.

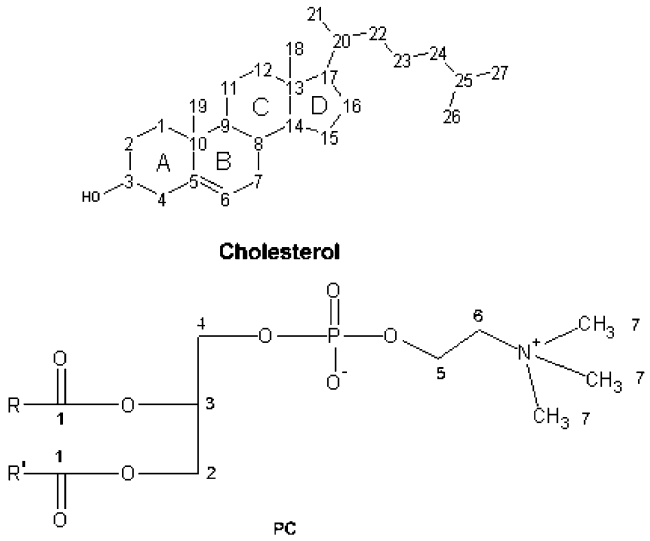

FIGURE 2: Chemical structures of cholesterol and phosphatidylcholine (PC). The numbering system for cholesterol follows IUPAC rules, while the numbering of PC is arbitrary and is used for purposes of identification only in the tables and figures. R and R′ are the acyl chains.

Circular Dichroism. CD spectra were recorded on an AVIV model 215 spectropolarimeter using a quartz cell with a path length of 0.1 cm. The cuvette was placed in a jacketed cell holder maintained at the desired temperature with circulating thermostatic fluid. The lipid was solubilized by incubation with the peptide.

Temperature scans were performed at a heating or cooling rate of either 1 or 2 °C/min, with a 30 s equilibration pause at each point for thermal equilibration. The ellipticity at 222 nm was measured as a function of temperature by starting at 25 °C, heating to 95 °C, and then cooling back to 25 °C to assess the reversibility of denaturation.

Tryptophan Fluorescence. Fluorescence emission spectra of 4F in the presence and absence of LUVs were recorded at 25 °C using an SLM Aminco Series II luminescence spectrometer. The excitation wavelength was 280 nm. Emission scans were recorded and processed for inner filter and instrumental corrections.

^1H NOESY MAS NMR. High-resolution MAS spectra were acquired using a spinning rate of 4 kHz in a Bruker DRX 500 NMR spectrometer. The probe temperature was 24 ± 1 °C. The two-dimensional NOESY spectra were obtained using mixing times of 50 and 300 ms. Resonances were assigned on the basis of their close similarity to literature values for phosphatidylcholine (*11*), cholesterol (*12*), and amino acid residues (*13*). The structures of the lipids that were used are given in Figure 2, numbered for the purposes of identification.

^{13}C CP/MAS NMR. A 4 mm zirconia rotor was placed in a Bruker Avance 300 spectrometer operating at 75.48 MHz for ^{13}C and equipped with CP/MAS capabilities. The spectra were referenced to an external standard of glycine crystals, assigning a chemical shift of 176.14 ppm for the carbonyl

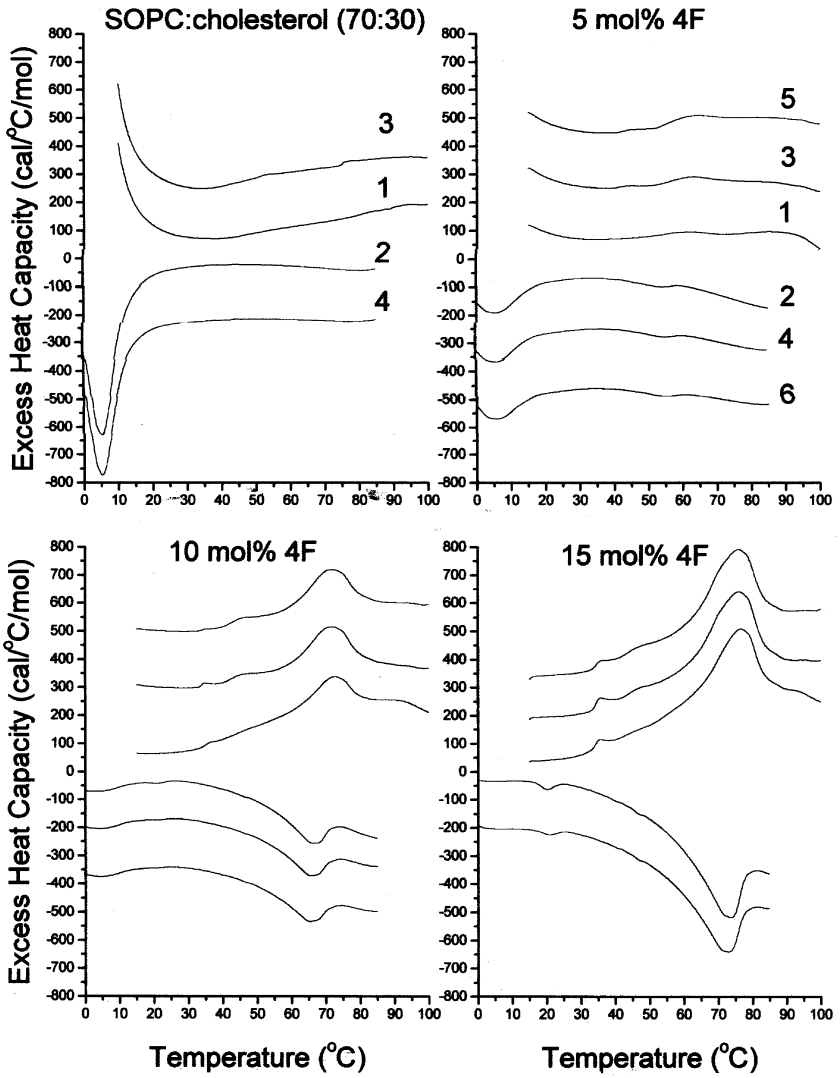

FIGURE 3: Differential scanning calorimetry of SOPC and cholesterol (7:3) with 0, 5, 10, or 15 mol % 4F. The scan rate was 2 K/min. The lipid concentration was 2.5 mg/mL in 20 mM PIPES, 1 mM EDTA, and 150 mM NaCl with 0.002% NaN_3 (pH 7.40). Sequential heating and cooling scans between 0 and 100 °C. Numbers are the order in which the scans were carried out, with scans 1, 3, and 5 being heating scans, each of which was followed by one of the cooling scans, scans 2, 4, and 6. Scans were displaced along the *y*-axis for clarity of presentation.

carbon. Samples were spun at 5 kHz. The temperature inside the rotor was 25 ± 1 °C. The power levels used for cross-polarization corresponded to a 4 μs $\pi/2$ pulse. The Hartmann−Hahn match was established on the sample of glycine. Continuous-wave decoupling at an increased power level was used during acquisition. Generally, each spectrum was obtained with 12 000 scans and processed with a line broadening of 1 Hz.

Direct Polarization. Single-pulse excitation with high-power proton decoupling was used with a 4 μs pulse for ^{13}C and the proton frequency optimized for decoupling. A recycle time of 5 s was used.

RESULTS

DSC. Three thermal transitions can be observed in some mixtures of SOPC, cholesterol, and 4F using DSC (Figures 3−5). The DSC curves are presented as the excess heat capacity per mole of cholesterol. The lowest transition temperature is ascribed to the gel to liquid crystalline transition of SOPC. This transition occurs near 0 °C, but its enthalpy, based on the concentration of SOPC, can be reasonably estimated from cooling scans. For pure SOPC (data not shown), the transition occurs at 5.5 °C on cooling at 2 K/min with a transition enthalpy of 4 kcal/mol (*14*). Previous results were presented per mole of SOPC (*14*), while in the case presented here, it is presented per mole of cholesterol. With pure SOPC without cholesterol, addition of 15 mol % 4F shifts the transition temperature on cooling to 7.9 °C and lowers the enthalpy to 1.5 kcal/mol (data not shown). The marked reduction in transition enthalpy indicates that the peptide decreases the energy difference between the gel state and the liquid crystalline state, likely by lowering the energy of the fluid phase. Addition of 30% cholesterol to SOPC lowers the transition enthalpy to 500 cal/mol of SOPC (*14*). Addition of 5, 10, and 15 mol % 4F to SOPC with 30% cholesterol results in a further lowering of the enthalpy to 270, 46, and 20 cal/mol of SOPC, respectively (Figure 3). At 40 or 50 mol % cholesterol, no transition is observed for the phospholipid in the presence of 4F (Figures 4 and 5).

Another transition observed in many of these scans is that from the polymorphic transition of anhydrous cholesterol.

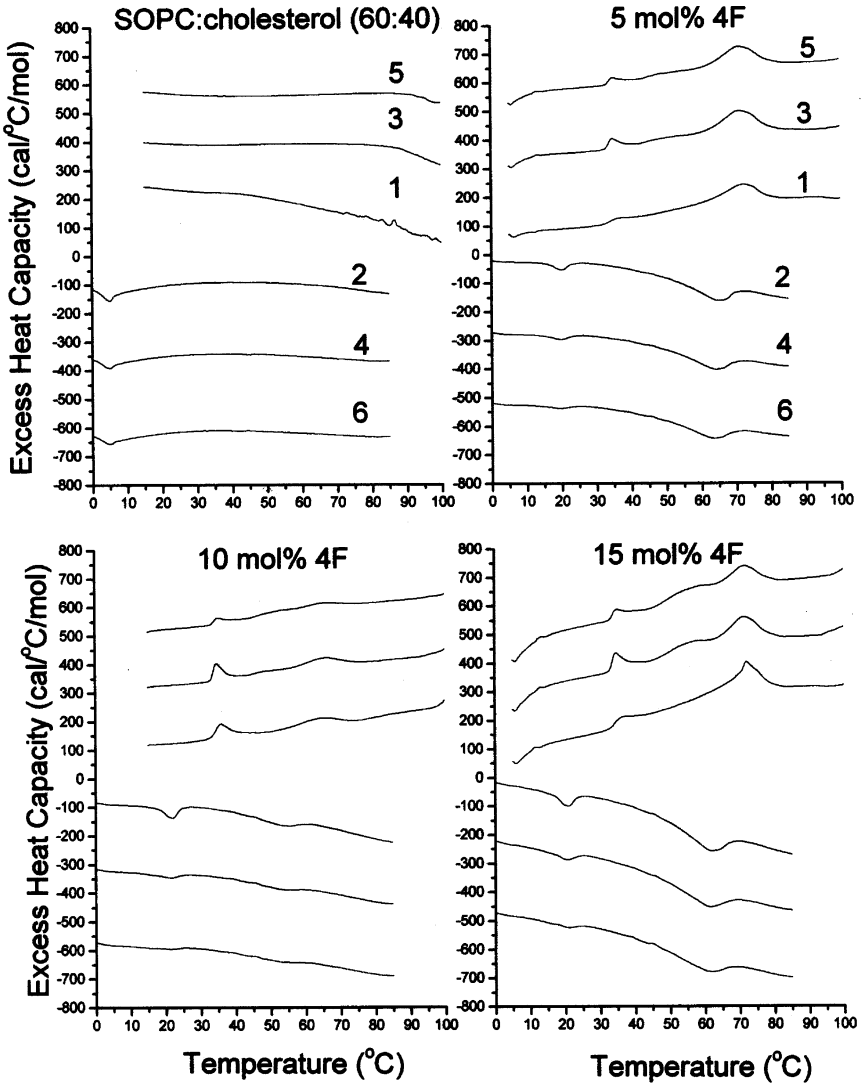

FIGURE 4: Differential scanning calorimetry of SOPC and cholesterol (6:4) with 0, 5, 10, or 15 mol % 4F. Other details were like those described in the legend of Figure 3.

For pure anhydrous cholesterol or anhydrous cholesterol mixed with phospholipids, this transition occurs at 37 °C on heating and 22 °C on cooling at the scan rate of 2 K/min used here (*15*). For the mixtures with 4F, the temperature of this transition is slightly shifted to 35 and 21 °C on heating and cooling, respectively. This may be an indication of the presence of a small amount of "impurity" in these crystals. However, the characteristic hysteresis of anhydrous cholesterol crystals is still observed. Six scans were run for each sample, three heating and three cooling. The average enthalpy observed for this transition is summarized in Table 1. In some samples, there was a decrease in the enthalpy of this transition in the final scans. This is noted in the table, and the lower values found in the later scans were not included in the average.

The highest temperature transition observed in the DSC scans corresponds to that of 4F. It occurs in the temperature range of ~55−75 °C, where a transition is also observed in the helical content of the peptide by CD (see below). The dehydration of crystals of cholesterol monohydrate also occurs in this temperature range, albeit somewhat higher. However, we do not believe any cholesterol monohydrate is formed during the time period of the DSC experiments. This is because the high transition temperature is readily reversible, unlike the dehydration of cholesterol monohydrate crystals (*16*). Furthermore, a similar transition is observed by DSC in samples of 4F in buffer or mixed with SOPC in the absence of cholesterol. The enthalpy of this transition on heating is ~5 kcal/mol of 4F and is ~25% greater on heating than on cooling. The transition temperature for the peptide in buffer is 60.3 °C on heating and 56.5 °C on cooling at a peptide concentration of 490 μM. CD results indicate that at this concentration the peptide in buffer has a conformation similar to that in lipid (see below). We would expect the enthalpy of the transition in buffer to be dependent on the peptide concentration, but this was not investigated. The transition temperature is increased by the presence of lipid and is not sensitive to the presence of cholesterol in the membrane (Table 2). The transition temperature is slightly lower on cooling than on heating.

CD. The circular dichroism of 4F in buffer is dependent on the concentration of the peptide (Figure 6, top). Addition of lipid to solutions of 4F at low concentrations augments the magnitude of the CD in the far-ultraviolet region. This is most dramatically seen when LPC is added to a solution of 19 μM 4F (Figure 6, middle). The spectra in the presence

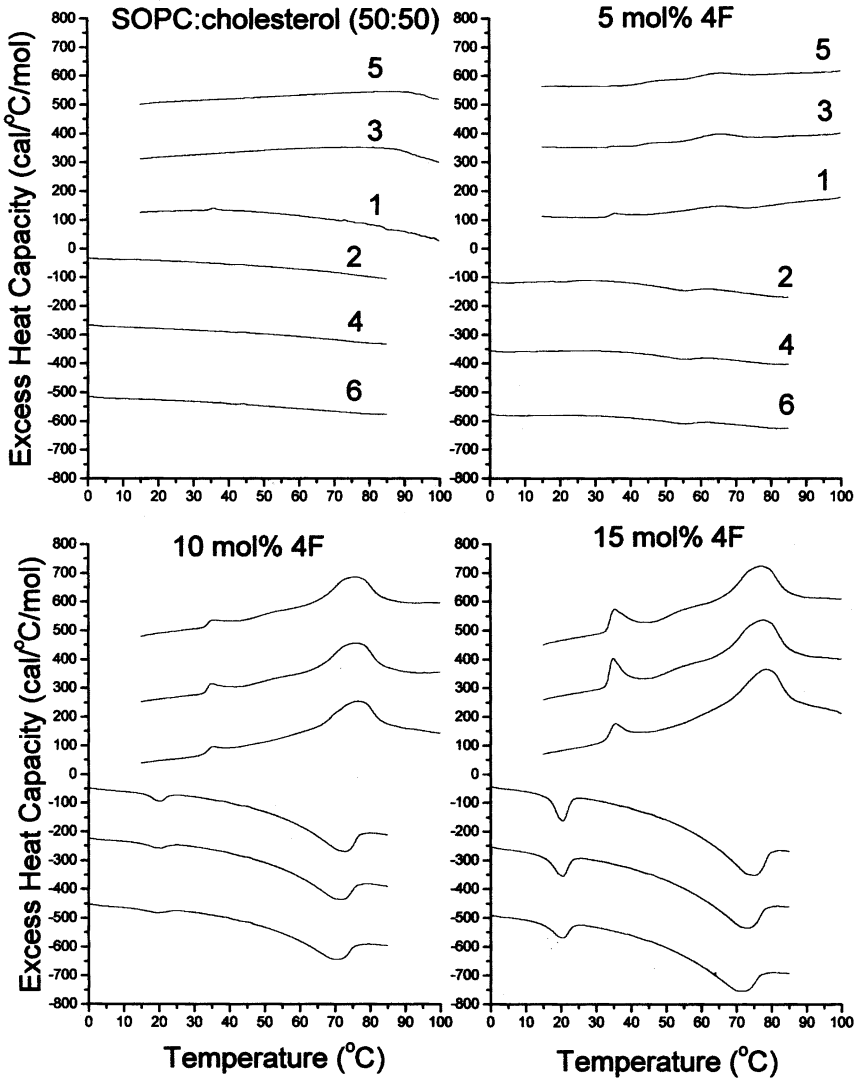

FIGURE 5: Differential scanning calorimetry of SOPC and cholesterol (1:1) with 0, 5, 10, or 15 mol % 4F. Other details were like those described in the legend of Figure 3.

Table 1: Enthalpy of the Polymorphic Transition of Anhydrous Cholesterol Crystals[a]

% cholesterol in SOPC	5% 4F	10% 4F	15% 4F
30	trace	13[b]	100[b]
40	120	150[b]	155[b]
50	50[b]	150	375

[a] Values in calories per mole of cholesterol determined from areas under the transitions at ~35 °C on heating and 21 °C on cooling shown in the DSC scans of Figures 3−5. [b] The enthalpy decreases after several heating and cooling scans.

Table 2: Transition Temperature (°C) for the Unfolding of 4F in the Presence of Lipid

% cholesterol in SOPC	5% 4F	10% 4F	15% 4F
Heating DSC Scans (transition at 60.3 °C in the absence of lipid)			
0	ND	ND	77
30	63	72	76
40	72	65	72
50	65	76	77
Cooling DSC Scans (transition at 56.5 °C in the absence of lipid)			
0	ND	ND	75.5
30	53	65	72
40	64	53	61
50	55	69	70

of lipid (Figure 6, bottom) are almost identical in the presence of SOPC and SOPC and cholesterol at ratios of 7:3 and 1:1 and are also independent of the peptide-to-lipid ratio in the range of 0.05−0.16 (not shown).

The temperature dependence of the spectrum shows a substantial loss of secondary structure on heating to 95 °C (Figure 7). The temperature at which the unfolding occurs is similar for the peptide in the presence of different lipid mixtures. However, in the absence of lipid, the peptide unfolds at a slightly lower temperature and the temperature and extent of unfolding are strongly dependent on peptide concentration. There is some hysteresis on heating and cooling, and at 25 °C, the peptide has somewhat less secondary structure after heating and cooling than before, particularly in the presence of lipid or for the peptide in buffer at low concentrations. This behavior is similar to that observed in DSC studies discussed above. Both CD and DSC show that this transition occurs at a higher temperature and with greater cooperativity in the presence of lipid.

Solubilization of Lipid and Peptide. Mixtures of SOPC, cholesterol, and 4F were centrifuged after the DSC experiments. In the presence of peptide, lipid is partially solubilized, presumably due to the formation of discoidal micelle particles (Figure 8). The peptide does not sediment in the absence of

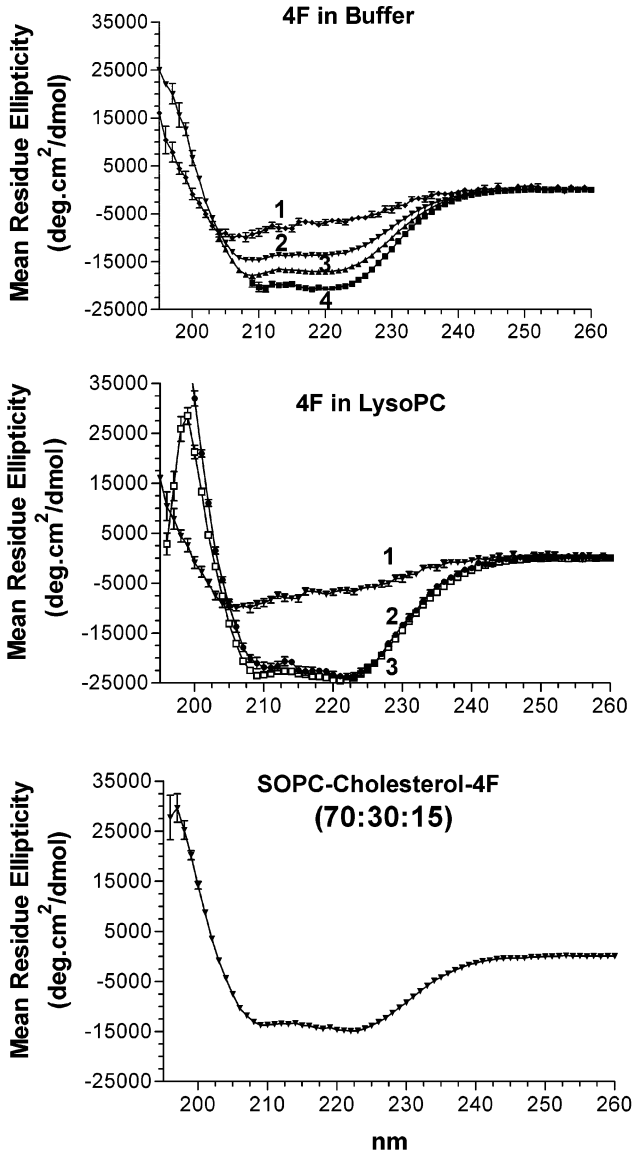

FIGURE 6: Circular dichroism spectra of 4F in buffer (top panel), in the presence of LPC (middle panel), and with SOPC and cholesterol (7:3) (bottom panel). The concentrations of 4F in buffer (top panel) are as follows: 19 μM for curve 1, 80 μM for curve 2, 165 μM for curve 3, and 330 μM for curve 4. In the middle panel, curve 1 shows 19 μM 4F in buffer for comparison, curve 2 shows 19 μM 4F with 10 mM LPC, and curve 3 shows 165 μM 4F with 10 mM LPC. The bottom panel is a spectrum of 136 μM 4F in a SOPC/cholesterol/4F mixture (70:30:15). The lipid was solubilized by the peptide, but the mixture was also sonicated to reduce the likelihood of scattering artifacts. This spectrum in the presence of lipid is representative of a number of similar spectra measured at different peptide concentrations and different SOPC-to-cholesterol ratios.

lipid; thus, all of the peptide in the pellet is bound to lipid. However, when lipid is present in the supernatant, soluble peptide can be free in solution or bound to solubilized lipid particles. In general, as more peptide is added, more SOPC is solubilized and less peptide is found in the pellet (Figure 8). Curiously, an increasing cholesterol concentration results in less solubilization of the lipid at 10% 4F, but more solubilization was observed at 15% 4F. At present, we cannot account for this change. The results for the partitioning of the lipid and peptide in the samples used for DSC indicate that in the case of the higher concentrations used for NMR the major fractions of the peptide and lipid are found in the pellet and not in the solubilized micellar form. This coincides with our finding of a bilayer-shaped static ^{31}P NMR powder pattern for this lipid mixture (see below).

Tryptophan Fluorescence. The fluorescence emission spectra of 4F were measured in buffer and in the presence of lipid (Figure 9). The emission maximum of the peptide in buffer is 340 nm but shifts to 333 nm in the presence of lipid, either with or without cholesterol. These values are somewhat lower than those for a series of 3F peptides, i.e., a series of amphipathic helical 18-amino acid peptides with identical sequences containing three Phe residues on the nonpolar face, that had emission at ~350 nm in buffer and ~338 nm in the presence of lipid (*17*). The results indicate that the Trp residue inserts into the bilayer. In addition, there is an approximately 2-fold increase in the emission intensity in the presence of SOPC in the absence of cholesterol, again indicating that the peptide interacts preferentially and inserts more deeply into bilayers not containing cholesterol. The ratio of intensities of Trp emission from 4F in buffer, 4F mixed with SOPC, and 4F mixed with SOPC and cholesterol is 1:1.3:2.0. The emission intensity is not sensitive to a change in the mole fraction of cholesterol from 0.3 to 0.5 or to the peptide:lipid ratio. It thus appears that in the presence of cholesterol the peptide is less deeply buried in the membrane. However, the Trp emission wavelength is not sensitive to the presence of cholesterol, indicating that the polarity of the Trp environment is not greatly altered.

^{1}H NOESY MAS NMR. Slices from the two-dimensional NOESY spectrum of 4F in the presence of POPC, at a 1:10 peptide-to-lipid ratio, are presented for the spectral region of the aromatic side chain resonances using a mixing time of 50 or 300 ms (Figure 10). ^{31}P NMR powder patterns demonstrated that all of the samples used for MAS studies were in a bilayer arrangement; although there was a very minor isotropic component in the spectra of 4F in the presence of POPC, this component was not present in the sample with POPC and cholesterol (not shown). The slices at 7.77 and 6.69 ppm from the two-dimensional NOESY spectrum of 4F in POPC (Figure 10) correspond to protons from the Trp and Tyr side chains, respectively. Both of these positions give rise to NOESY cross-peaks with the methylene protons of the acyl chain having a negative sign, indicating rapid motion. The resonance at 7.02 ppm has a strong positive cross-peak with the CH_2CCO protons, while the 7.13 ppm resonance has a positive cross-peak with the methylene protons of the acyl chain. These resonances likely come from the side chain of Tyr. The spectra taken with mixing times of 50 and 300 ms appear to be qualitatively similar, indicating that spin diffusion does not play a major role in affecting the intensities of the cross-peaks. These findings indicate that the peptide inserts into the bilayer of POPC but does not access the center of the bilayer; i.e., there are no cross-peaks with the terminal methyl groups of the acyl chain. The Tyr residue is adjacent to a Phe residue in the linear sequence of 4F (Figure 1). If there is stacking between these aromatic residues or with others that are spatially close as a result of folding, it would result in a shift to a lower frequency (upfield) of the Tyr resonances as a result of ring current effects. Thus, the CH group ortho to the OH group has a resonance at 6.69 ppm compared to the random coil value of 6.86 ppm, and the meta CH group of Tyr that is usually at 7.15 ppm appears in these spectra at 7.02 ppm. The ortho

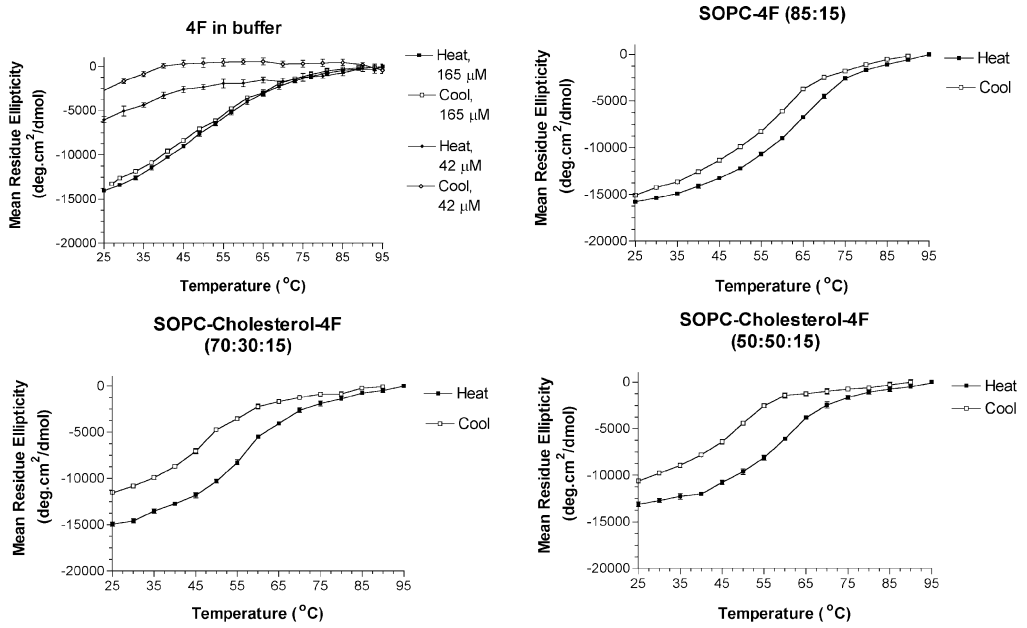

FIGURE 7: Temperature dependence of the mean residue ellipticity at 222 nm of 4F in buffer and in the presence of lipid as indicated. For each run, there is a heating cycle (■) and a cooling cycle (□). The spectra in buffer are very dependent on peptide concentration. Results for runs at 42 and 165 μM are shown. The concentration of peptide in the presence of lipid was 90 μM.

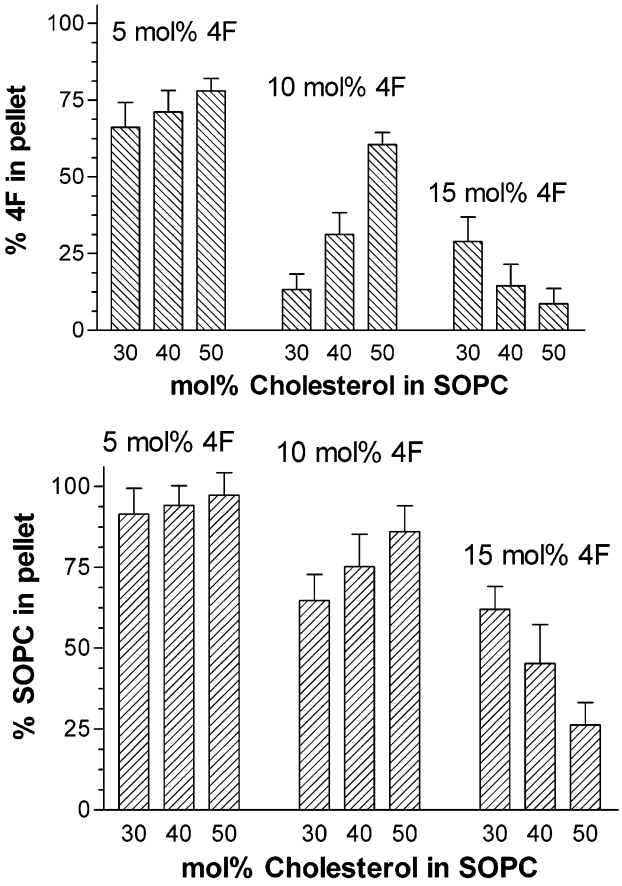

FIGURE 8: Solubilization of the peptide and lipid in mixtures of 4F and MLV of SOPC with 0.3, 0.4, or 0.5 mole fraction cholesterol, each containing 5, 10, and 15 mol % peptide, after the series of DSC runs shown in Figures 3−5. Error bars are the standard error of the mean of experiments repeated three times.

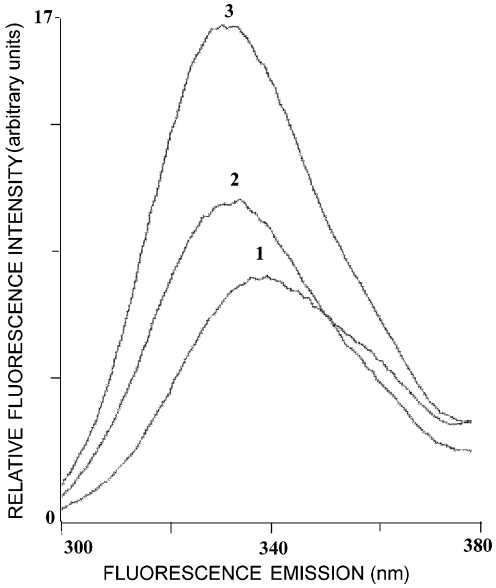

FIGURE 9: Fluorescence emission spectra of 4F: (1) 60 μM 4F in buffer, (2) 45 μM 4F mixed with SOPC and cholesterol (1:1) at a lipid-to-peptide ratio of 10, and (3) 45 μM 4F mixed with SOPC at a lipid-to-peptide ratio of 10.

CH group would likely be closer to the membrane interface, being adjacent to the OH group of Tyr. This position has more molecular motion than the meta CH group that is more deeply buried in the membrane and hence gives rise to negative NOEs. The other group that gives rise to negative NOEs comes from the Trp residue that lies between two polar Lys resides in the helical wheel projection (Figure 1). This group is therefore also likely to be less buried in the membrane and hence would have greater motion, as indicated by the negative sign for the NOEs.

The NOESY slices from the spectra of 10 mol % 4F in bilayers of POPC and cholesterol (1:1) are qualitatively different. With a mixing time of 50 ms, there are virtually no off-diagonal peaks (Figure 11, left side). High expansion is required to barely detect some signals above the noise level. However, all of the aromatic protons show cross-peaks with aliphatic residues when a mixing time of 300 ms is used (Figure 11, right side). Again in the case of the Tyr residue (6.80 ppm slice), the NOESY peaks are negative for

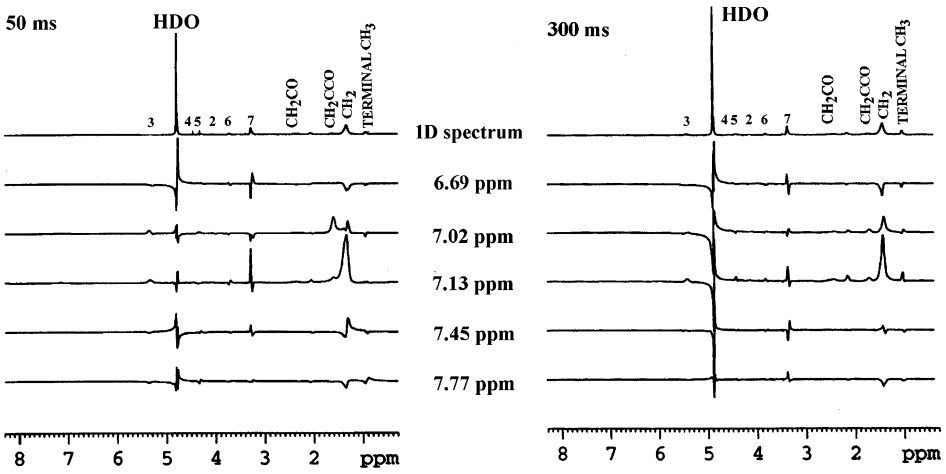

FIGURE 10: One-dimensional slices from the MAS ^{1}H NOESY spectrum at the chemical shifts of the aromatic protons of a sample of POPC containing 10 mol % 4F. The mixing times were 50 (left) and 300 ms (right). Top spectra are conventional one-dimensional proton spectra of the samples. Resonance assignments are indicated on the top spectrum using the numbering system given in Figure 2.

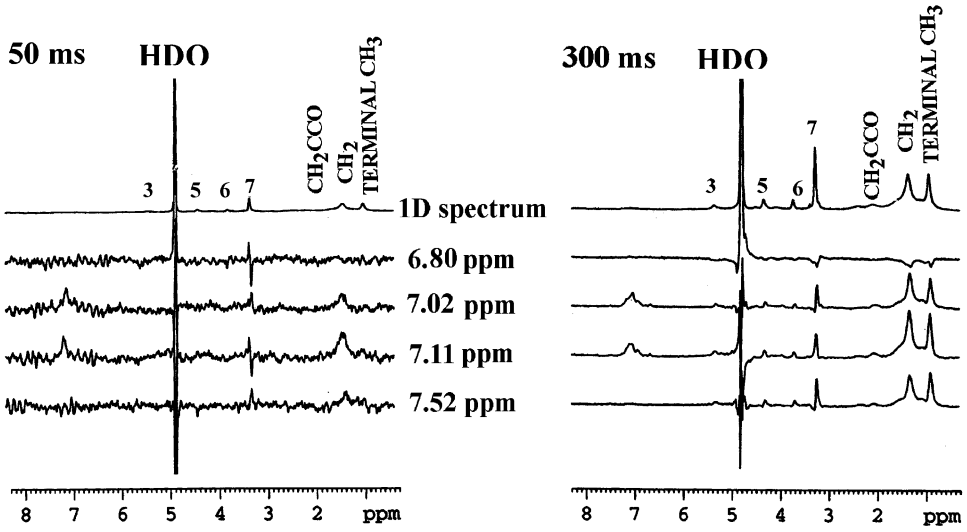

FIGURE 11: One-dimensional slices from the MAS ^{1}H NOESY spectrum at the chemical shifts of the aromatic protons of a sample of POPC and cholesterol (1:1) containing 10 mol % 4F. The mixing times were 50 (left) and 300 ms (right). Top spectra are conventional one-dimensional proton spectra of the samples. Resonance assignments are indicated on the top spectrum using the numbering system given in Figure 2.

the ortho protons on the ring, indicative of a high degree of motion. The nonlinear dependence of the signal intensity on mixing time is evidence of spin diffusion.

Interaction of 4F with lipid can also be assessed by monitoring the changes in the chemical shifts of the lipid resonances upon introduction of the peptide (Table 3). These changes in chemical shifts may arise from ring current effects as well as from changes in the polarity of the environment. In the case of ^{1}H MAS/NMR, only changes in the spectrum of the phospholipid can be assessed, since resonances are not observed from protons of cholesterol in these lipid mixtures (*11*) and the lower concentration of peptide makes it difficult to discern its resonances. The largest change in chemical shift caused by addition of the peptide to POPC in the absence of cholesterol is the shift of the CH_2CO resonance of the acyl chain to a lower frequency (Table 3). This result suggests that the aromatic groups of 4F penetrate into the bilayer, below the interfacial region, in the absence of cholesterol. In contrast, in a 1:1 mixture of POPC and cholesterol, the largest changes in chemical shift occur for protons in the lipid headgroup and shifts caused by 4F for these protons are greater in the presence than in the absence of cholesterol (Table 3). These results indicate that 4F is largely at the interface of membranes containing cholesterol; however, the peptide is able to penetrate more deeply into bilayers of POPC that are devoid of cholesterol.

Table 3: Changes in ^{1}H Chemical Shifts of Lipid Resonances Induced by 4F

	chemical shift difference[a] (ppm)	
resonance	POPC	1:1 POPC/cholesterol
glycerol C2 (3)	0	0.02
glycerol C3 (4)	0.01	0.03
choline α (5)	0.01	0.02
glycerol C1 (2)	0.005	0.01
choline β (6)	0.01	0.02
quaternary CH_3 (7)	0.015	0.02
CH_2CO	0.04	0.01
CH_2	0.01	0.02
terminal CH_3	0.01	0.02

[a] Chemical shift differences are between that of lipid alone and in the presence of 10 mol % 4F. A positive sign corresponds to a shift in the resonance to a lower frequency caused by the peptide.

Table 4: ^{13}C Chemical Shift Differences of Lipid Resonances

assignment[a]	chemical shift (ppm)	1:1 POPC/cholesterol with or without 4F[b]
acyl C═O	174	0.19
cholesterol C5	142	0.22
acyl C═C	130.1	0.16
acyl C═C	129.6	0.14
cholesterol C6	121	0.13
glycerol C2 (3)	71	0.26
choline β (6)	66	0.15
glycerol C3 (4)	64	0.10
choline α (5)	60	0.16
cholesterol C14/17	57	0.17
quaternary CH_3 (7)	54	0.17
cholesterol C9	51	0.06
cholesterol C13	43	0.17
cholesterol C24	40	0.13
cholesterol C10	37	0.17
acyl C2	35	0.17
cholesterol C2	31	0.25
cholesterol C16	29	−0.028
cholesterol C25	28	−0.14
cholesterol C19/21	20	−0.37
acyl terminal methyl	14	0.12

[a] Numbers in parentheses correspond to the numbering shown in Figure 2. [b] Chemical shift differences are between that of lipid alone and in the presence of 10 mol % 4F. A positive sign corresponds to a shift in the resonance to a lower frequency caused by the peptide.

^{13}C MAS/NMR. Resonances from both POPC and cholesterol can be observed with ^{13}C MAS/NMR. Two methods were used to measure the ^{13}C spectra. One is CP/MAS NMR that utilizes cross polarization from protons to carbon atoms to increase the intensity of the ^{13}C signals (not shown). The efficiency of cross polarization is greatest for positions that are relatively rigid, giving higher-intensity CP/MAS signals. The other method is direct polarization that should provide a measure of the number of all carbon atoms, provided that the delay time is sufficiently long compared with the spin−lattice relaxation time. Rigid structures may require delay times that are so long that they are impractical to attain.

First, we compare changes in the ^{13}C chemical shifts of various carbon atoms of the lipid caused by the addition of 4F to POPC and cholesterol (1:1) (Table 4). Resonances of both the phospholipid and cholesterol are altered by the peptide, suggesting that there is no preferential interaction of the peptide with one lipid component or the other. Resonances from atoms expected to be deep within the bilayer are also shifted as a result of peptide penetration. We suggest this is a consequence of molecular motion causing transient contact and/or of changes in lipid packing.

We have also compared the peak intensities from MAS spectra of POPC and cholesterol (1:1) using both CP and DP/MAS and compared the DP/MAS spectra with and without 4F (Table 5). The CH_3 peak of the choline headgroup has an intensity in CP/MAS that is much lower than expected for the number of carbon atoms. This indicates that this group has a high mobility. Several of the resonances exhibit similar intensities via DP/MAS in the presence and absence of 4F. These include the C═O group, one of the acyl C═C groups (at 129.5 ppm), the CH_3 group of the choline N-$(CH_3)_3$, and the terminal CH_3 group of the lipid acyl chain (the cholesterol C18 is a special case and will be discussed below). Other resonances arise from more rigid positions and do not give DP/MAS intensities that correspond to the number of protons.

Table 5: ^{13}C Peak Intensities for Mixtures of POPC and Cholesterol (1:1) Containing 10 mol % 4F

			relative observed intensities		
assignment	chemical shift (ppm)	no. of C atoms	CP/MAS with 10% 4F	DP with 10% 4F	DP lipid alone[e]
C═O	173.8	2	0.50	0.98	0.94
cholesterol C5	141.9	1	0.25	0.21	0.45
acyl C═C	129.9	1[a]	1.04	0.65	0.82
acyl C═C	129.5	1[a]	0.96	0.93	0.95
cholesterol C6	120.5	1	0.48	0.29	0.54
quaternary CH_3	54.3	3[b]	0.32	3.0	3.0
terminal CH_3	14.1	2	1.95	1.91	2.08
crystalline cholesterol monohydrate C18	13.7	*c*	ND[d]	0.16	0
cholesterol C18	12.6	*c*	1.37	0.68	0.71
crystalline cholesterol monohydrate C18	11.9	*c*	0.40	ND[d]	0

[a] Relative to the total number of C═C groups set to 2.0 for CP/MAS. [b] Relative to the number of quaternary CH_3 groups set to 3.0 for DP/MAS. [c] Sum of these three values should equal 1. [d] Not determined because signal not sufficiently above the noise level. [e] Taken from ref *18* using a delay time of 100 s. Intensities from spectra using a delay time of 5 s were similar.

These positions, the C5 and C6 double bond position of cholesterol and the acyl chain C═C group at 129.5 ppm, have even lower intensities in the presence of 4F, indicating that this peptide rigidifies certain regions of the bilayer. Finally, the C-18 peak of cholesterol has a chemical shift of 12.6 ppm when dissolved in a membrane, but is split into peaks at 11.9 and 13.7 ppm when present as crystals of cholesterol monohydrate. From the intensities of these peaks, one can estimate (*18*) the percent of total cholesterol that is in the crystalline form, 20% (*18*). This compares with 11% crystalline anhydrous cholesterol found in fresh samples using DSC with SOPC (Table 1). The estimates of crystalline cholesterol levels from NMR and DSC are in the same range, although they are not identical. Factors such as the increased length of time for measurement and conversion of the anhydrous cholesterol crystals and the much higher concentration of lipid used for the NMR may contribute to the observed difference.

DISCUSSION

Compared with other peptides that lower the solubility of cholesterol in bilayers of phosphatidylcholine (*14*, *19*), peptide 4F is particularly potent in promoting the formation of cholesterol crystals. Even with cholesterol mole fractions as low as 0.3, cholesterol crystals are formed in the presence of higher concentrations of 4F (Table 1). In some cases, the enthalpy of the polymorphic transition of anhydrous cholesterol decreases with repeated scanning between 0 and 100 °C. A factor that likely contributes to this effect is the fact that the conformational transition of the peptide on heating is not completely reversible (Figure 7). Also, some pure lipid systems exhibit this kind of metastability, such as mixtures of SOPC and cholesterol, that forms metastable cholesterol crystals at 0.7 mole fraction of cholesterol (*20*).

The peptide *N*-acetyl-LWYIK-amide (*14*) and the myristoylated protein, NAP-22 (*19*), also promote the formation of cholesterol crystals in lipid mixtures of cholesterol and PC. However, there is a qualitative difference in the mechanism by which the segregation of cholesterol crystals is promoted by 4F. NAP-22 does not interact with liposomes

of pure PC (*19*, *21*), and DSC studies demonstrate that *N*-acetyl-LWYIK-amide promotes the formation of domains enriched in SOPC in which the enthalpy of the phospholipid transition is greater in the presence of peptide than in its absence (*14*). In contrast, 4F interacts strongly with pure PC. The ^{1}H NOESY spectra indicate that 4F inserts more deeply into membranes composed of only PC than into bilayers of PC containing cholesterol. This is the opposite of the situation with *N*-acetyl-LWYIK-amide (*14*). Peptide 4F markedly reduces the enthalpy of SOPC, while both NAP-22 and *N*-acetyl-LWYIK-amide have virtually no effect on the enthalpy of pure PC. In the case of 4F, SOPC-enriched domains also contain the peptide and therefore have broadened transitions with lower enthalpies that are not detected. Thus, 4F gives rise to the formation of cholesterol-rich domains by interacting with PC and stabilizing domains devoid of cholesterol. In contrast, *N*-acetyl-LWYIK-amide (*14*) and NAP-22 (*19*, *22*) bind preferentially to cholesterol-rich domains to stabilize them. Polyunsaturated acyl chains also promote the formation of cholesterol-rich domains by not interacting with cholesterol (*23*). Curiously, both 4F peptides (*2*, *3*) and certain polyunsaturated fatty acids (*24*−*26*) have antiatherogenic properties in humans. It remains to be determined if there is some commonality in the action of these diverse substances.

The enthalpy of denaturation of 4F is ∼6 kcal/mol both in the presence and in the absence of lipid. The helical content of 4F in the presence of lipid was estimated to be 60% at 25 °C, based on analysis of the CD spectrum (*27*). At 95 °C, there is essentially no helical structure remaining. We therefore estimate that of 18 amino acid residues in the peptide, an average of 10.8 residues lose their helical structure when the peptide is heated. This would then correspond to an enthalpy for breaking the helix of 0.55 kcal/mol per residue. The enthalpy of formation of an α-helix in water has been estimated to be in the range of 0.9−1.3 kcal/mol per residue (*28*−*34*). The value is somewhat lower, 0.7 kcal/mol per residue, in the more hydrophobic environment of 7 M trifluoroethanol (*35*). Estimates for helix formation in the binding of amphipathic helical peptides to SUVs or to LUVs have been determined using isothermal titration calorimetry to be 0.5−0.6 kcal/mol per residue for a peptide corresponding to a mitochondrial presequence (*36*) and 0.7−0.8 kcal/mol per residue for antimicrobial peptide magainin II (*37*). The heat of reaction of a peptide related to 4F, i.e., *N*-acetyl-18A-amide, is 1.3 kcal/mol in liposomes (*38*), similar to that of the human plasma apolipoproteins, apo A-II and apo C-III, associating with phospholipids (*39*). Our estimate of the enthalpy required to break the helical structure of 4F is comparable to other estimates. However, it should be kept in mind that the estimates determined by isothermal titration calorimetry for the other peptides also include the energy changes caused by peptide−lipid interactions, while in our DSC measurements, the peptide may remain on the lipid before and after unfolding. Furthermore, the two types of measurements are based on data from different temperatures, and if ΔC_p is not zero, there will be a temperature dependence of the observed enthalpy. In addition, the thermal transition monitored by CD for the unfolding of 4F occurs at a somewhat lower temperature than the calorimetric transition, suggesting that the transition observed by DSC arises from processes in addition to peptide unfolding. The secondary structure content, as determined by CD, is increased by both peptide−lipid and peptide−peptide interactions. The relative enthalpic contributions of these two kinds of interactions are not known, but are likely to be different and could contribute to the differences observed in the unfolding transition of 4F as measured by CD and DSC.

We have previously shown that 4F is particularly potent in inducing the quenching of DPH-PC in bilayers of POPC (*17*). This is an indication that the peptide, as a consequence of its deeper insertion, allows a deeper penetration of water into the membrane. Our NMR studies indicate insertion of the aromatic amino acid side chains of 4F past the membrane interface. This would cause a disruption of the packing of the phospholipid and allow deeper penetration of water. In a biological plasma membrane that contains cholesterol, there would be the additional feature that cholesterol would be depleted from the regions where the peptide binds. This would also loosen the packing of the lipid, allowing deeper water penetration. This phenomenon has been used to explain the anti-inflammatory activity of 4F (*17*). Furthermore, the sequestering of cholesterol into domains may also facilitate its transfer to cholesterol-rich domains of the plasma membrane, such as caveolae, where it can transfer into lipoprotein particles (*40*). Thus, the molecular nature of the interaction of 4F with membranes can provide a mechanism for the antiatherogenic actions of this peptide both in inhibiting inflammatory processes and in reverse cholesterol transport.

REFERENCES

1. Navab, M., Anantharamaiah, G. M., Reddy, S. T., Van Lenten, B. J., Hough, G., Wagner, A., Nakamura, K., Garber, D. W., Datta, G., Segrest, J. P., Hama, S., and Fogelman, A. M. (2003) Human apolipoprotein AI mimetic peptides for the treatment of atherosclerosis, *Curr. Opin. Invest. Drugs 4*, 1100−1104.
2. Garber, D. W., Datta, G., Chaddha, M., Palgunachari, M. N., Hama, S. Y., Navab, M., Fogelman, A. M., Segrest, J. P., and Anantharamaiah, G. M. (2001) A new synthetic class A amphipathic peptide analogue protects mice from diet-induced atherosclerosis, *J. Lipid Res. 42*, 545−552.
3. Navab, M., Anantharamaiah, G. M., Hama, S., Garber, D. W., Chaddha, M., Hough, G., Lallone, R., and Fogelman, A. M. (2002) Oral administration of an Apo A-I mimetic peptide synthesized from D-amino acids dramatically reduces atherosclerosis in mice independent of plasma cholesterol, *Circulation 105*, 290−292.
4. Glomset, J. A. (1968) The plasma lecithins:cholesterol acyltransferase reaction, *J. Lipid Res. 9*, 155−167.
5. Van Lenten, B. J., Wagner, A. C., Anantharamaiah, G. M., Garber, D. W., Fishbein, M. C., Adhikary, L., Nayak, D. P., Hama, S., Navab, M., and Fogelman, A. M. (2002) Influenza infection promotes macrophage traffic into arteries of mice that is prevented by D-4F, an apolipoprotein A-I mimetic peptide, *Circulation 106*, 1127−1132.
6. Egashira, M., Gorbenko, G., Tanaka, M., Saito, H., Molotkovsky, J., Nakano, M., and Handa, T. (2002) Cholesterol modulates interaction between an amphipathic class A peptide, Ac-18A-NH_2, and phosphatidylcholine bilayers, *Biochemistry 41*, 4165−4172.
7. Gorbenko, G., Handa, T., Saito, H., Molotkovsky, J., Tanaka, M., Egashira, M., and Nakano, M. (2003) Effect of cholesterol on bilayer location of the class A peptide Ac-18A-NH_2 as revealed by fluorescence resonance energy transfer, *Eur. Biophys. J. 32*, 703−709.
8. Datta, G., Chaddha, M., Hama, S., Navab, M., Fogelman, A. M., Garber, D. W., Mishra, V. K., Epand, R. M., Epand, R. F., Lund-Katz, S., Phillips, M. C., Segrest, J. P., and Anantharamaiah, G. M. (2001) Effects of increasing hydrophobicity on the physical-chemical and biological properties of a class A amphipathic helical peptide, *J. Lipid Res. 42*, 1096−1104.
9. Ames, B. N. (1966) Assay of inorganic phosphate, total phosphate and phosphatases, *Methods Enzymol. 8*, 115−118.

10. Privalov, G., Kavina, V., Freire, E., and Privalov, P. L. (1995) Precise scanning calorimeter for studying thermal properties of biological macromolecules in dilute solution, *Anal. Biochem. 232*, 79−85.
11. Forbes, J., Bowers, J., Shan, X., Moran, L., Oldfield, E., and Moscarello, M. A. (1988) Some new developments in solid-state nuclear magnetic resonance spectroscopy studies of lipids and biological membranes, including the effects of cholesterol in model and natural systems, *J. Chem. Soc., Faraday Trans. 84*, 3821−3849.
12. Guo, W., and Hamilton, J. A. (1996) ^{13}C MAS NMR studies of crystalline cholesterol and lipid mixtures modeling atherosclerotic plaques, *Biophys. J. 71*, 2857−2868.
13. Arnold, M. R., Kremer, W., Ludemann, H. D., and Kalbitzer, H. R. (2002) ^{1}H NMR parameters of common amino acid residues measured in aqueous solutions of the linear tetrapeptides Gly-Gly-X-Ala at pressures between 0.1 and 200 MPa, *Biophys. Chem. 96*, 129−140.
14. Epand, R. M., Sayer, B. G., and Epand, R. F. (2003) Peptide-induced formation of cholesterol-rich domains, *Biochemistry 42*, 14677−14689.
15. Epand, R. M., Bach, D., Borochov, N., and Wachtel, E. (2000) Cholesterol crystalline polymorphism and the solubility of cholesterol in phosphatidylserine, *Biophys. J. 78*, 866−873.
16. Loomis, C. R., Shipley, G. G., and Small, D. M. (1979) The phase behavior of hydrated cholesterol, *J. Lipid Res. 20*, 525−535.
17. Datta, G., Epand, R. F., Epand, R. M., Chaddha, M., Kirksey, M. A., Garber, D. W., Lund-Katz, S., Phillips, M. C., Hama, S., Navab, M., Fogelman, A. M., Palgunachari, M. N., Segrest, J. P., and Anantharamaiah, G. M. (2004) Aromatic Residue Position on the Nonpolar Face of Class A Amphipathic Helical Peptides Determines Biological Activity, *J. Biol. Chem.* (in press).
18. Epand, R. M., Bain, A. D., Sayer, B. G., Bach, D., and Wachtel, E. (2002) Properties of Mixtures of Cholesterol with Phosphatidylcholine or with Phosphatidylserine Studied by ^{13}C Magic Angle Spinning Nuclear Magnetic Resonance, *Biophys. J. 83*, 2053−2063.
19. Epand, R. M., Maekawa, S., Yip, C. M., and Epand, R. F. (2001) Protein-induced formation of cholesterol-rich domains, *Biochemistry 40*, 10514−10521.
20. Epand, R. M., Hughes, D. W., Sayer, B. G., Borochov, N., Bach, D., and Wachtel, E. (2003) Novel properties of cholesterol-dioleoylphosphatidylcholine mixtures, *Biochim. Biophys. Acta 1616*, 196−208.
21. Maekawa, S., Sato, C., Kitajima, K., Funatsu, N., Kumanogoh, H., and Sokawa, Y. (1999) Cholesterol-dependent localization of NAP-22 on a neuronal membrane microdomain (raft), *J. Biol. Chem. 274*, 21369−21374.
22. Khan, T. K., Yang, B., Thompson, N. L., Maekawa, S., Epand, R. M., and Jacobson, K. (2003) Binding of NAP-22, a Calmodulin-Binding Neuronal Protein, to Raft-like Domains in Model Membranes, *Biochemistry 42*, 4780−4786.
23. Brzustowicz, M. R., Cherezov, V., Zerouga, M., Caffrey, M., Stillwell, W., and Wassall, S. R. (2002) Controlling Membrane Cholesterol Content. A Role for Polyunsaturated (Docosahexaenoate) Phospholipids, *Biochemistry 41*, 12509−12519.
24. Bhatnagar, D., and Durrington, P. N. (2003) Omega-3 fatty acids: their role in the prevention and treatment of atherosclerosis related risk factors and complications, *Int. J. Clin. Pract. 57*, 305−314.
25. Hirafuji, M., Machida, T., Hamaue, N., and Minami, M. (2003) Cardiovascular protective effects of n-3 polyunsaturated fatty acids with special emphasis on docosahexaenoic acid, *J. Pharmacol. Sci. 92*, 308−316.
26. Yaqoob, P., and Calder, P. C. (2003) N-3 polyunsaturated fatty acids and inflammation in the arterial wall, *Eur. J. Med. Res. 8*, 337−354.
27. Sreerama, N., Venyaminov, S. Y., and Woody, R. W. (1999) Estimation of the number of α-helical and *β*-strand segments in proteins using circular dichroism spectroscopy, *Protein Sci. 8*, 370−380.
28. Chou, P. Y., and Scheraga, H. A. (1971) Calorimetric measurement of enthalpy change in the isothermal helix−coil transition of poly-L-lysine in aqueous solution, *Biopolymers 10*, 657−680.
29. Hermans, J., Jr. (1966) Experimental free energy and enthalpy of formation of the α-helix, *J. Phys. Chem. 70*, 510−515.
30. Ooi, T., and Oobatake, M. (1991) Prediction of the thermodynamics of protein unfolding: the helix−coil transition of poly(L-alanine), *Proc. Natl. Acad. Sci. U.S.A. 88*, 2859−2863.
31. Rialdi, G., and Hermans, J., Jr. (1966) Calorimetric heat of the helix−coil transition of poly-L-glutamic acid, *J. Am. Chem. Soc. 88*, 5719−5720.
32. Scholtz, J. M., Qian, H., York, E. J., Stewart, J. M., and Baldwin, R. L. (1991) Parameters of helix-coil transition theory for alanine-based peptides of varying chain lengths in water, *Biopolymers 31*, 1463−1470.
33. Scholtz, J. M., Marqusee, S., Baldwin, R. L., York, E. J., Stewart, J. M., Santoro, M., and Bolen, D. W. (1991) Calorimetric determination of the enthalpy change for the α-helix to coil transition of an alanine peptide in water, *Proc. Natl. Acad. Sci. U.S.A. 88*, 2854−2858.
34. Scholtz, J. M., and Baldwin, R. L. (1992) The mechanism of α-helix formation by peptides, *Annu. Rev. Biophys. Biomol. Struct. 21*, 95−118.
35. Luo, P., and Baldwin, R. L. (1997) Mechanism of helix induction by trifluoroethanol: a framework for extrapolating the helix-forming properties of peptides from trifluoroethanol/water mixtures back to water, *Biochemistry 36*, 8413−8421.
36. Wieprecht, T., Apostolov, O., Beyermann, M., and Seelig, J. (2000) Interaction of a mitochondrial presequence with lipid membranes: role of helix formation for membrane binding and perturbation, *Biochemistry 39*, 15297−15305.
37. Wieprecht, T., Beyermann, M., and Seelig, J. (2002) Thermodynamics of the coil−α-helix transition of amphipathic peptides in a membrane environment: the role of vesicle curvature, *Biophys. Chem. 96*, 191−201.
38. Gazzara, J. A., Phillips, M. C., Lund-Katz, S., Palgunachari, M. N., Segrest, J. P., Anantharamaiah, G. M., and Snow, J. W. (1997) Interaction of class A amphipathic helical peptides with phospholipid unilamellar vesicles, *J. Lipid Res. 38*, 2134−2146.
39. Massey, J. B., Gotto, A. M., Jr., and Pownall, H. J. (1979) Contribution of α helix formation in human plasma apolipoproteins to their enthalpy of association with phospholipids, *J. Biol. Chem. 254*, 9559−9561.
40. Fielding, C. J., and Fielding, P. E. (2003) Relationship between cholesterol trafficking and signaling in rafts and caveolae, *Biochim. Biophys. Acta 1610*, 219−228.

BI049786U